Capturing the spatiotemporal dynamics of task-initiated thoughts with combined EEG and fMRI

Lucie Bréchet[1,2], Denis Brunet[2,3], Gwénaël Birot[4], Rolf Gruetter[1,3], Christoph M. Michel[2,3] and João Jorge[1]

[1] Laboratory for Functional and Metabolic Imaging, EPFL, Lausanne, Switzerland
[2] Functional Brain Mapping Laboratory, Fundamental Neuroscience Dept., University Geneva, Switzerland
[3] Biomedical Imaging Research Center (CIBM), Lausanne, Geneva, Switzerland
[4] EEG-BCI Facility - Fondation Campus Biotech Geneva

Abstract

When at rest, our mind wanders from thought to thought in distinct mental states, portrayed by William James as the brief flights and perchings of a bird. Despite the marked importance of ongoing mental processes, in cognitive neuroscience and clinical contexts alike, it is challenging to capture and relate these states to specific cognitive contents. In this work, we employed ultra-high field functional magnetic resonance imaging (fMRI) and high-density electroencephalography (EEG) to study the ongoing thoughts of participants instructed to retrieve self-relevant past episodes for periods of 20s. These task-initiated, participant-driven activity patterns were compared to a distinct condition where participants performed serial mental arithmetic operations, thereby shifting from self-related to self-unrelated thoughts. BOLD activity mapping revealed selective activity changes across conditions, namely in temporal, parietal and occipital areas ("posterior hot zone"), evincing their role in integrating the re-experienced past events into conscious representations during memory retrieval. Functional connectivity analysis showed that these regions were organized in two major subparts of the default mode network, previously associated to "scene-reconstruction" and "self-experience" subsystems. EEG microstate analysis allowed studying these brief participant-driven thoughts in the millisecond range. While the microstate topographies were found stable across conditions, the occurrence and duration of specific microstates were selectively modulated. EEG source analysis revealed similar spatial distributions between the sources of these microstates and the regions identified with fMRI. These findings imply a functional link between BOLD activity changes in regions related to a certain mental activity and the temporal dynamics of mentation, and support growing evidence that specific fMRI networks can be captured with EEG as repeatedly occurring, integrated brief periods of synchronized neuronal activity, lasting only fractions of seconds.

Significance

We investigated the spatiotemporal dynamics of large-scale brain networks related to specific conscious thoughts. We demonstrate here that instructing participants to direct their thoughts to either episodic autobiographic memory or to mental arithmetic modulates distinct networks both in terms of highly spatially-specific BOLD signal oscillations as well as fast sub-second dynamics of EEG microstates. The combined findings from the two modalities evince a clear link between hemodynamic and electrophysiological signatures of spontaneous brain activity, capturing the occurrence of thoughts that last for fractions of seconds, repeatedly occurring over time as integrated coherent activities of specific large-scale networks.

Introduction

The occurrence of spontaneous conscious thoughts is difficult to grasp experimentally (1–3). Spontaneous mentation is neither random nor meaningless (4–7), however how to precisely capture the wandering mind and attribute it to specific cognitive thoughts, is yet unclear. Functional magnetic resonance imaging (fMRI) as well as electroencephalography (EEG) studies have previously related resting-state activity to cognitive processes mainly indirectly by using post-scan questionnaires (8–10) or by asking participants about their ongoing thoughts during the spontaneous mentation (11–14). The self-reports can be assessed with probe-caught methods, in which participants are asked about their ongoing thoughts at certain intervals (15–18) or with self-caught methods, in which participants report mind-wandering that they notice by themselves(19). The striking similarities found by comparing the spatial distributions of large-scale networks specific to self-reported thoughts and those initiated by experimental tasks (20–23), contribute to the wide debate about the content of spontaneous mental activity at rest (4, 5, 7, 12, 24–31). Numerous studies on spontaneous mentation using both task as well as rest conditions showed that a specific network, i.e. the default mode network (DMN), becomes involved when we think about ourselves (5, 8, 20, 26). The DMN was first described as de-activated during cognitive experiments (32, 33). However, further investigations revealed a number of self-related processes (e.g. episodic autobiographical memory, internally directed thoughts, self-projections) that strongly activate the DMN (18, 20, 34–36).

Time-resolved fMRI studies previously demonstrated that the resting state networks (RSNs) spontaneously fluctuate in and out of spatially and temporally overlapping correlations (37–45), indicating that functional dynamics of resting state activity are not continuous, but rather partitioned into distinct epochs. This observation corroborates the prevailing concept that spontaneous mental activity is discontinuous and parsed into a series of conscious states that

manifest discrete spatiotemporal patterns of neuronal activity. Terms such as "pulses of consciousness" (46), "perceptual frames" (47), "neuronal workspace" (48, 49), "heteroclinic chanel" (50), or "structure flow on manifolds" (51) describe the various concepts of brain states' meta-stability (for review see (52–54)). However, despite much progress in dynamic resting-state functional neuroimaging, by the sluggish nature of the hemodynamic response to neuronal activity, fMRI methods have only a limited capacity to capture these states(38). Indeed, in order to efficiently execute mental processes, the large-scale networks have to dynamically re-organize on *sub-second* temporal scales (29, 41). EEG microstate analysis allows to investigate the fast temporal dynamics of large-scale neural networks and to access information about the functional organization of spontaneous mentation in time (54, 55). Previous evidence shows that EEG microstates reflect brief epochs of synchronized activity of spontaneous mentation that persist for tens of milliseconds (54, 56, 57). Moreover, the occurrence and duration of EEG microstates determine the quality of spontaneous mentation, and as such could represent the basic building blocks of conscious mental processes (15, 58). EEG microstates thus qualify as the electrophysiological segmentation of ongoing mental activity into short-lasting brain states (54, 58, 59). Yet, despite several efforts using simultaneous EEG-fMRI (60–63), the functional and neurophysiological relation between EEG microstates and fMRI resting states is far from clear (54).

The goal of this study was to capture the occurrence of spontaneous thoughts within specific, externally-controlled cognitive domains, combining ultra-high field fMRI and high-density EEG recordings to obtain both hemodynamic and electrophysiological signatures with high functional sensitivity. Recent works have explored novel experimental designs based on task-initiated spontaneous activity, whereby participants are asked to think freely, but within specific cognitive tasks (20–23). These approaches have yielded promising insights into the cognitive underpinnings of spontaneous thoughts, and are well suited to the recording and analysis of continuous activity with techniques like EEG and fMRI. Following this approach, we collected high-resolution 7T fMRI and 64-channel EEG data from 15 healthy participants during uninstructed spontaneous mentation (hereafter termed "rest condition") or while they focused their thoughts for periods of 20sec on either episodic, self-related memories ("memory condition"), or arithmetic calculations ("math condition") (Fig. 1). Consistent with cognitive tasks that require working memory and direct the attention outside of the self (33, 64, 65), we chose the math condition in order to selectively de-activate DMN regions, which we expected to become active in episodic memory retrieval (66–69). The spatial architecture of task-initiated fMRI resting brain activity was mapped in terms of the fractional amplitude of low frequency

fluctuations (fALFF) (70). To probe functional changes specific to the distinct cognitive domains, we compared the spatial distribution of these local activity changes, as well as their organization in large-scale networks, across conditions. We then examined the fast temporal organization of the brain's large-scale network dynamics, using the EEG microstate approach. Specifically, we focused on the most basic characteristics of the EEG microstate temporal dynamics: their duration, their frequency of occurrence and their transition probabilities. Finally, using a newly developed, precise method to localize the sources of broadband scalp topographies (*SI Appendix,* SMethod2), we demonstrate that we can reliably estimate the brain networks generating the EEG microstates and relate them to the fMRI RSNs.

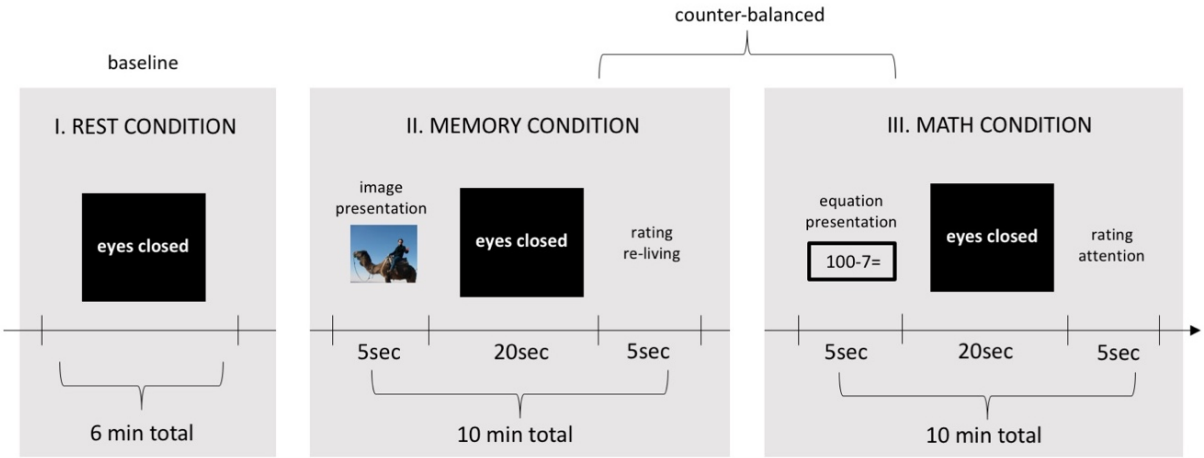

Fig. 1. Experimental paradigm.
15 healthy participants (30.5±5.5years) took part in both high-density 64-channel EEG and 7T-fMRI sessions in three distinct conditions during eyes closed: rest (6min), mentally retrieving personal past episodes (10min), and mental arithmetic (10min). Before the scanning, all participants performed a classical autobiographical memory questionnaire (ABMQ)[9] in order to select vividly remembered images for the memory retrieval condition. Before each of the memory retrieval and mental arithmetic trials, participants saw a personal image/calculation for 5sec, after which they closed their eyes and had to either retrieve the event or continue to subtract the numbers (20sec). After each trial, there were 5sec for a control question to answer: *"How much did you relive the original event?"* for memory task and *"How much attention did you pay to the calculation?"* for the memory task (scale 1 =not at all to 4=fully).

Results

Condition-specific changes in fMRI activity across brain regions.

To identify changes in spontaneous activity across different brain regions during the two stimulus-initiated thoughts, i.e. math and memory conditions, the fractional amplitude of low-frequency fluctuations (fALFF) (70) was mapped, serving as a model-free measure of local BOLD activity (71). Having obtained a fALFF estimate for each brain voxel of each fMRI run

and participant, these values were then statistically compared between conditions on the group level using topological false-discovery rate (FDR) inference (72) (T>2.20, α=5%). Condition-specific fALFF changes were thereby found for several cortical and subcortical brain regions.

The regions with significantly higher brain activity during the memory compared to the math condition were consistent to those previously described in episodic memory studies (65, 73–79) (Fig. 2a). These included the core brain areas of the episodic memory retrieval network found in the parietal, the medial temporal, the prefrontal and occipital lobes. Most dominantly, we found activity in the lateral part of the parietal lobe: bilaterally the supramarginal gyrus (lrSMG, BA40) and the right angular gyrus (rAG, BA39) of the inferior parietal lobe (IPL). Activity was also found in the medial part of the parietal lobe: the left precuneus (lPCu, BA7), the dorsal part and the ventral part of the posterior cingulate cortex/retrosplenial cortex (dPCC, BA23; vPCC/RSc, BA31). In the temporal lobe we found bilaterally-increased activity in the parahippocampal gyri (lrPHG, BA28,35,36) and the right inferior temporal gyrus (rITG, BA21). Significant activity was also found in the right inferior frontal gyrus (rIFG, BA45), and bilaterally in the lateral occipital gyri (lrLOCG, BA19). Importantly, comparing the fALFF estimates in these brain regions to the non-instructed rest condition (i.e. considered as baseline) revealed that some of the memory-math differences were due to a stronger increase in BOLD activity during the memory compared to math condition (areas included lrPHG and dPCC), while other changes were due to increased BOLD activity during the memory and decreased BOLD activity during the math conditions. Areas de-activated during math compared to rest included rAG, lrSMG, lrLOCG, PCu and vPCC/RSc. (Fig. 2b). Conversely, we also identified a set of brain areas active during the math compared to the memory condition (including the frontoparietal operculum/insula, the inferior parietal sulcus, pre/post central gyrus and dorsal part of the anterior cingulate cortex, the superior frontal/temporal gyrus) that have been previously associated to mental arithmetic tasks and frontoparietal control network (FPCN) in general (80–86) (*SI Appendix,* Figs. S1a and S1b).

Condition-specific networks found with fMRI functional connectivity analysis.

The brain regions that demonstrated significant BOLD activity changes between the memory and math conditions, as identified by the fALFF analysis, were then analyzed further in terms of their functional connectivity. The functional connectivity between each pair of regions was estimated as the average Pearson correlation between the time course of every voxel in the first region with that of every voxel in the second region. This method was also applied to each region paired with itself, thereby yielding a measure of homogeneity within the region. These

connectivity values were organized in matrices, and the regions were re-ordered according to their correlation profiles. The connectivity analysis revealed two distinct networks within the regions that had displayed stronger activity during the memory condition (Figs. 2c and 2d). Network I. included the vPCC/RSc, lrPHG, lrLOCG, rITG and lPCu. This network was strikingly similar to a previously described subsystem of the DMN (20, 87), which becomes involved during constructions of mental scenes (hereafter termed "scene-reconstruction subsystem"). Network II. comprising the rIFG, rAG, lrSMG, dPCC and lateral lrOCG, closely matched a previously defined subsystem of the DMN (20, 87), which becomes active when participants engage in self-relevant cognitive processes and reflect on their current mental states (hereafter termed "self-experience subsystem"). Compared to the non-instructed rest condition, both networks displayed strong increases in connectivity amidst their respective regions, while remaining uncorrelated to each other. Our results support the multi-component aspects of DMN, showing that different regions of this network behave differently and form functionally distinct subsystems based on the cognitive function involved (87–89).

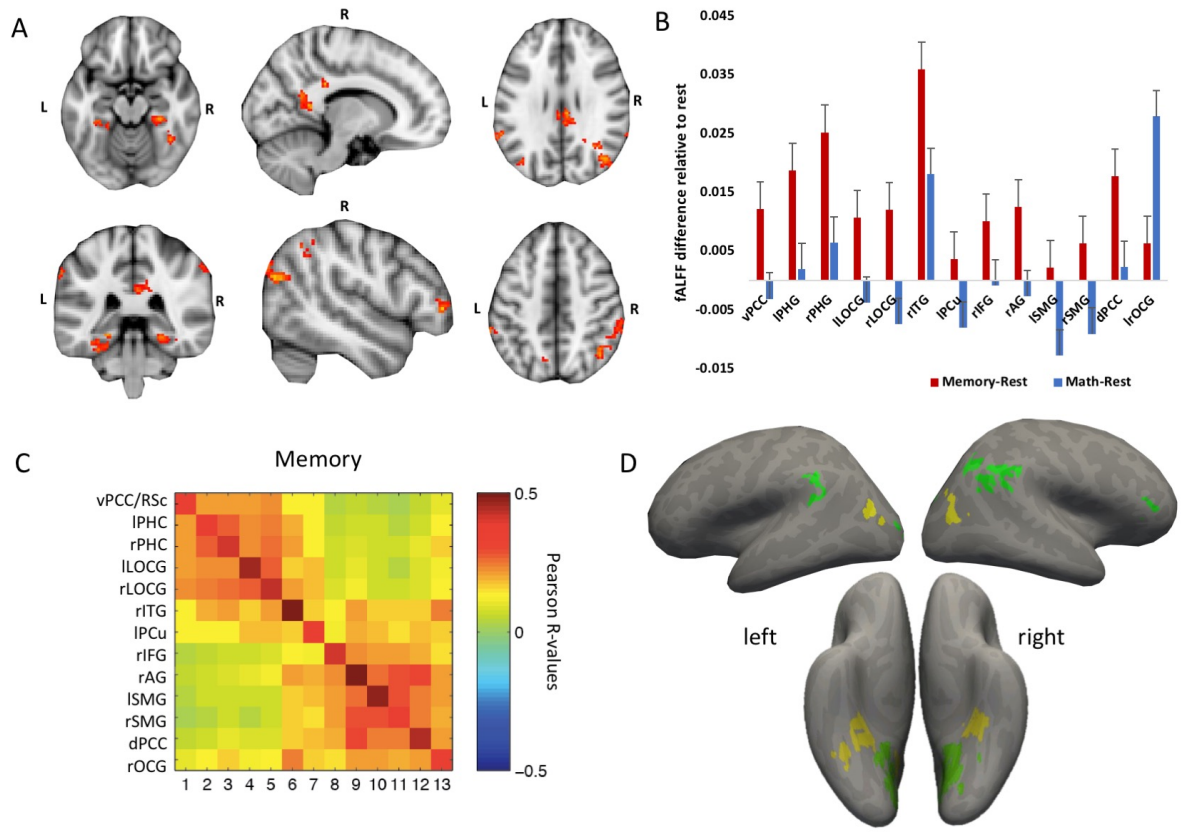

Fig. 2. Memory-specific changes in fMRI activity and fMRI functional connectivity memory sub-networks.

A. fMRI fALFF analysis. T-test of fALFF for memory > math condition revealed stronger activity in lrSMG, rAG, lrLOCG, lPCu, dPCC, vPCC/RSc, lrPHG, rITG, rIFG. T-score

threshold: T>2.20; FDR-corrected for multiple comparisons (5%). **B. Areas of stronger activity in the memory, compared to math condition.** Some of the memory-math differences were due to a stronger increase in BOLD activity during the memory compared to math condition (areas included lrPHG and dPCC), while other changes were due to increased BOLD activity during the memory and decreased BOLD activity during the math conditions. **C. Connectivity analysis.** Network I. included the vPCC/RSc, lrPHG, lrOCG, rITG and lPCu, which we called "scene-reconstruction subsystem". Network II. comprised the DLPFC, rAG, lrSMG, and dPCC, called "self-experience subsystem". **D. Sub-networks of the connectivity analysis.** Regions were also projected onto a surface template for better visualization.

Differences in duration and occurrence of EEG microstates.

Having found a high spatial organization of functionally connected networks during the memory vs. math conditions using fMRI, we then examined the fast temporal organization of these large-scale networks. First, we identified the most dominant EEG microstate maps for each of the three conditions (i.e. math, memory and rest conditions) using a *k*-means cluster analysis. The optimal number of clusters, determined by a meta-criterion (*SI Appendix,* SMethod1) appeared to be six for each condition. The topographies of these six maps were strikingly similar between the three conditions and resembled those previously described in the literature (54). We ordered the microstate maps according to their highest spatial correlation across conditions (i.e. math, memory, rest) and labeled them from A-F states (90, 91) (Fig. 3a). Statistical comparison of the underlying brain sources that generated these microstates confirmed highly similar networks between the corresponding maps in the three conditions (*SI Appendix,* Table S1). We then fitted the maps back to the original EEG of each participant and labelled each time point with the microstate that had highest spatial correlation (Fig. 3b). This procedure allowed us to determine the mean duration of each microstate in the three conditions, and how often the microstates occurred independent of their duration.

We expected that microstates activated by our task-initiated paradigm would last longer and occur more often during the corresponding math and memory conditions. Taking a conservative p-value smaller than 0.0001, the ANOVA analyses for each microstate indeed revealed that two states (i.e. microstates C and D) significantly differed in their duration depending on the condition (Fig. 3c) and three states (i.e. microstates B, C and D) significantly differed in their occurrence (Fig. 3d). Microstate B was specific to the memory condition as it significantly increased in occurrence compared to math as well as compared to rest conditions (both $p<0.0001$). Also microstate C was significantly increased in duration and occurrence in the memory compared to the math condition. Interestingly, the increase of microstate C in the memory condition was due to a decrease of this state in the math condition compared to rest

(p<0.001), reminding us of the decrease of BOLD activity in math compared to rest. Thus, microstate C was dominating during both rest and memory conditions, while it was strongly diminished when participants were instructed to focus on mental calculations. Finally, microstate D significantly increased in occurrence and duration in the math compared to the memory (p<0.001) and the rest (p<0.0001) conditions.

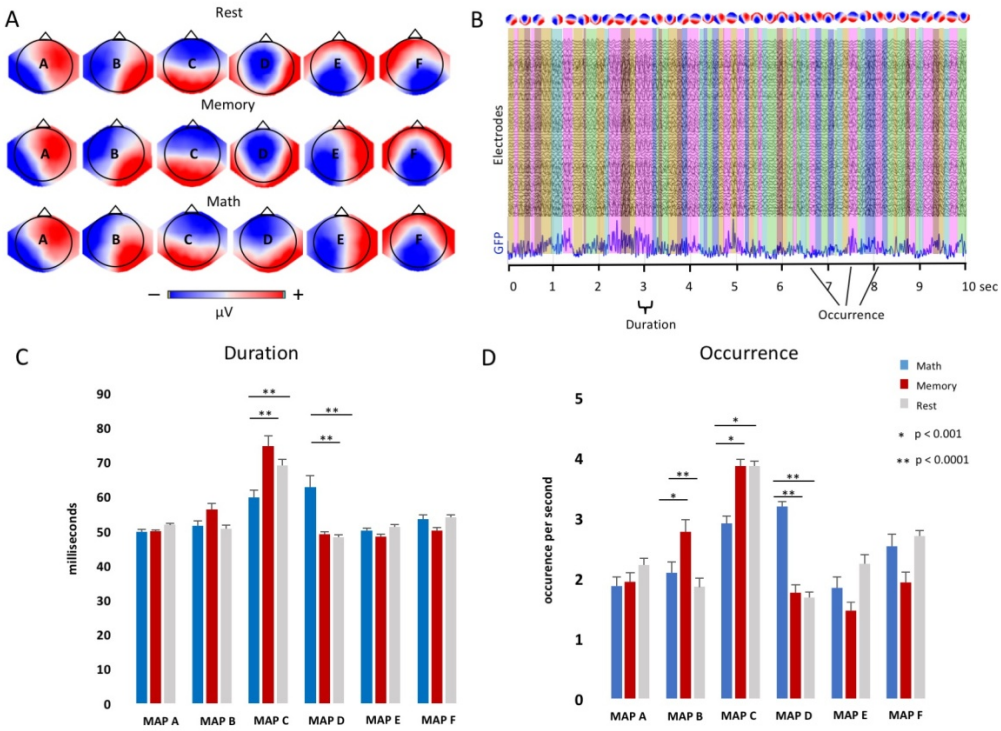

Fig. 3. Temporal dynamics of EEG microstates.

A. The six microstates identified by k-means cluster analysis across subjects in the three conditions (rest, memory and math). Notice the high spatial similarity between conditions. The six maps are labeled according to their resemblance with microstate maps described in the literature. **B.** A representative period of 10-sec EEG with eyes closed after picture presentation is shown (traces of 64 electrodes and Global Field Power (GFP) trace). Back-fitting the 6 microstate maps derived from the cluster analysis shows the chunking of the EEG into segments of various durations (40-100 ms) covered by one of the microstate maps (indicated by different colors). Note that for visualization purposes some short segments were smoothed out in this figure. **C.** Mean and standard error of the duration of each of the microstates in each condition. Post-hoc tests were performed when the ANOVA revealed significant condition differences at p<0.0001. This was the case for microstate map C and map D: Microstate C was significantly shorter and microstate D significantly longer in the math condition compared to memory and rest. **D.** Occurrence of the six microstates in the three conditions (number of microstates per second). Significant ANOVAs (p<0.0001) were found for microstates B, C, and D. As for the duration, microstate C occurred less and microstate D more often in the math condition compared to rest and memory (p<.0001). Concerning microstate B, an increased occurrence was found for memory compared to math (p<.001) and rest (p<.0001).

Source localization of the EEG microstates.

To estimate networks underlying each microstate we inverted the original data of each subject into source space using a distributed linear inverse solution (92). For standardization, a modified z-transform was applied for each solution point across all three conditions (*SI Appendix,* Methods). We then averaged the estimated activity across all time points that were labelled with the same microstate maps for each subject and each condition. The brain regions underlying the six microstate maps confirmed and extended previous efforts (91, 93) in source localization of microstates (Fig. 4). In detail, microstate A showed left-lateralized activity in the superior temporal gyrus (STG), the medial prefrontal cortex (MPFC) and the OCG. Microstate B showed main activity in OCG and in the medial part of the parietal cortex in the PCu/RSc. The sources of microstate C were located bilaterally in the lateral part of the parietal cortex including both the SMG and AG. The sources of microstate D showed main activity bilaterally in the IFG, dACC, and superior parietal lobule (SPL)/intraparietal sulcus(IPS). Strongest activity for microstate E was found in the right MPFC. Finally, microstate F showed bilateral activity in the MPFC. All areas that showed activity above 95 percentiles are depicted.

Remarkably, the network underlying microstate C, which occurred more often and lasted longer in the memory compared to the math condition, largely overlapped with the lateral parietal areas of the memory retrieval network from the fMRI analyses. Particularly, we attributed these areas to "self-experience subsystem", which is linked with the subjective experience of the self and one's mental states (20, 65, 94). Correspondingly, the brain areas underlying microstate B, which selectively increases in occurrence during the memory condition, overlapped with the medial parietal areas of the memory network detected in the fMRI analyses. We attributed these areas to the "scene-reconstruction subsystem" (20, 95–97). Brain areas underlying microstate D included areas generally attributed to the frontoparietal control network (FPCN) (65, 89, 98, 99).

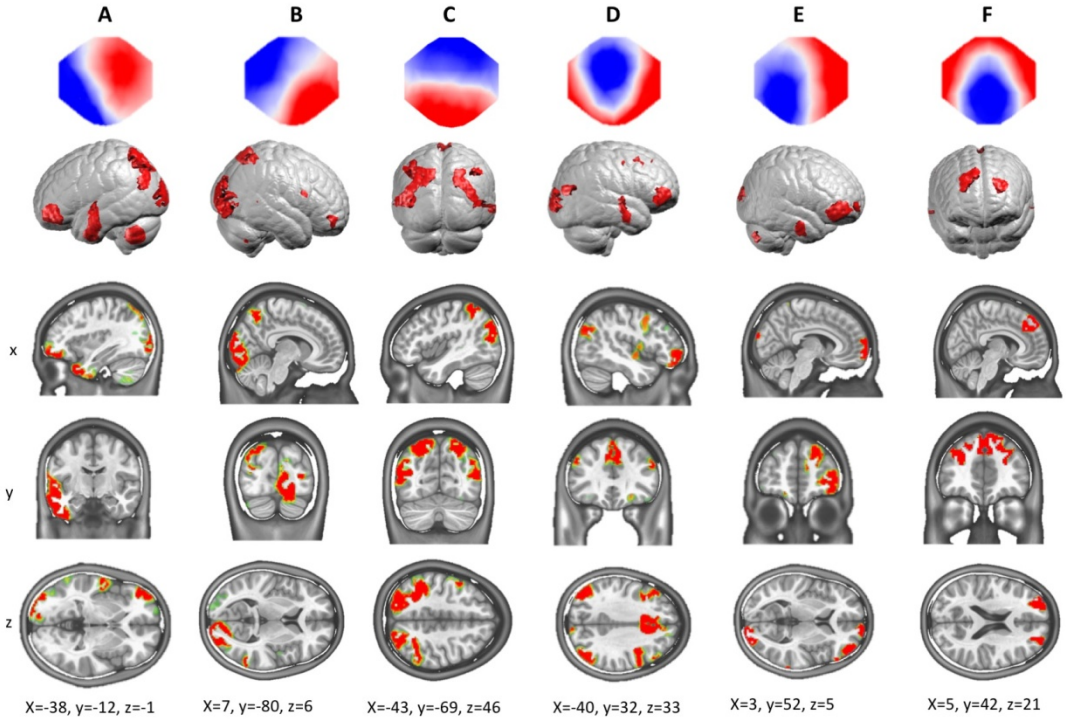

Fig. 4. Source localization of EEG microstates.

The EEG of each participant and condition were subjected to a distributed linear inverse solution and normalized across time. The source maps of all time points that were labelled with the same microstate map were then standardized across time and averaged within participants. The mean sources across subjects in the memory condition are illustrated here (for individual source maps per condition see *SI Appendix,* SFigs. 2-4). Areas with activity above 95 percentiles are shown. Notice the strong activity of the superior parietal lobe for microstate C (strong presence in memory and rest) and the frontoparietal activity for microstate D (strong presence in math).

Transition probabilities between microstates.

Following the interpretation that the two dominating microstates in the memory condition reflect brain networks that are involved in mental scene reconstruction (microstate B) and self-relevant cognitive processes (microstate C), we hypothesized whether participants alternate between these two kinds of thoughts across time. In order to answer this question, we considered the normalized transition probabilities to account for their different occurrence levels between microstate C and D and compared them to all other possible transitions. Indeed, we found that specifically and only in the memory condition, the transition from microstate C to microstate B was significantly more frequent than the transition from any other state ($p < .05$) and that microstate B transitions significantly more often over to microstate C than to any other state (all $p < 0.0001$) **(Fig. 5)**. Likewise, microstate C was significantly more often followed by microstate B than microstates A, D or E (all $p<.01$), but not F. These dominant transitions

between microstate B and C were not observed in the math nor in the rest conditions.

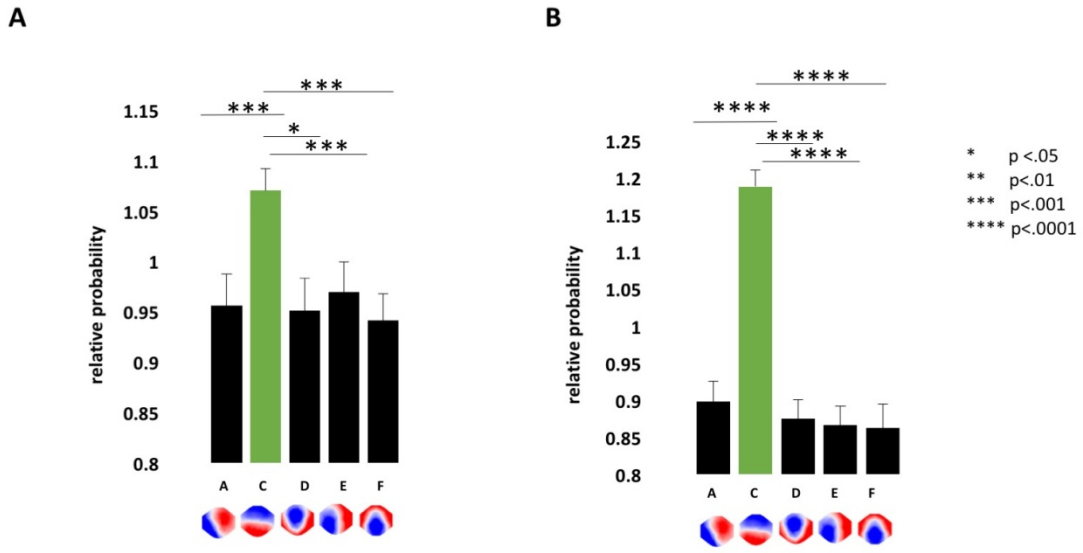

Fig. 5. Markov chain transition probabilities.

We calculated the transition probabilities from each microstate to any other using Markov chains. The observed probabilities were divided by the expected probabilites to account for the variability in occurrence of the states. In the memory condition, we found that microstate B was significantly more often preceded **(A)** and followed **(B)** by microstate C than any of the other microstates. This transition behavior was not found during rest or when participants performed mental arithmetic operations.

Discussion

To capture the occurrence of any conscious experience, "qualia", and to directly investigate the cognitive processes operating during mind-wandering, it is crucial to better control the spontaneous thoughts of participants (12, 100). Mind-wandering is not always spontaneous as the stream of our thoughts is often triggered by external stimuli, emotions and memories, which altogether play a crucial part in our daily experience (28). Individuals often direct the flow of thoughts they are immersed in by these external experiences. Consequently, mind-wandering is often task-related (10, 17). Based on this fact, and in line with other recent studies (20–23), we here initiated periods of spontaneous mentation with brief presentations of external stimuli and instructed participants to close their eyes and internally direct their thoughts to either self-related photographs or self-unrelated arithmetic operations. Using high-resolution whole-brain 7T fMRI, we directly compared activity of brain areas whenever participants engaged in the memory- or math- initiated mentation. The main regions observed in the memory condition comprise the IPL and MTL structures. Numerous studies have previously identified these regions as the core of the episodic memory retrieval network (73–76, 88). Traditionally, since the

discovery of densely amnesic patients, the MTL structures have been regarded as essential for long-term memory formation, allowing us to remember past experiences and to retrieve acquired knowledge (101–107). Intriguingly, conscious experience has been reported as preserved after bilateral lesions to the MTL structures (108, 109). In contrast to the MTL structures, extensive evidence from patient lesion and brain stimulation studies suggests that the IPL plays a key role in integrating vivid details of personally experienced events into conscious representations during memory retrieval (65, 94, 110–113). The subjective experience of perceiving a scene, recognizing a face, hearing a sound or reflecting on the experience itself presents a complex interplay between memory, attention and consciousness (65, 114, 114–116). Tulving (117, 118) defined the underlying ability to re-experience the subjective sense of self in the past and to mentally project oneself into the future, i.e. the autonoetic consciousness, as the crucial aspect of episodic memory retrieval. Evidence across lesion studies, stimulation and recording studies consistently point to the posterior regions, including temporal, parietal and occipital areas ("posterior hot zone") as playing a direct role in specifying the contents of consciousness (99, 100, 119, 120). Our current findings are also in line with a recent study (121) where we confirmed the contribution of the IPL, especially the AG, to the subjective, first-person perspective re-experience of self-relevant, vivid past episodes.

Our next aim was to capture the sub-second changes in temporal dynamics of brain states during the memory or math-initiated spontaneous mentation. Brain activity constantly fluctuates in and out of different mental states that are stable for fractions of seconds, whereby mind-wandering thoughts tend to remain fixed on a single theme or topic. Only one epoch or state of conscious content can be considered at a time (122, 123). It is assumed that the EEG microstates capture these states that last for around 80-200 milliseconds only (58, 59). Using high-density whole-brain EEG, we indeed observed modulations of duration and occurrence of particular microstates by the instructed thoughts. We found that microstate C lasted longer and occurred more often during the memory compared to math instructed thoughts, while microstate D revealed the reverse behavior (i.e. increased during the math condition compared to the memory condition). Additionally, microstate B increased in occurrence during the memory compared to math and rest conditions.

The topographies of these three microstates strongly resemble three of the four canonical microstates previously described in the literature (for reviews see (54, 124)). Studies on large cohorts showed that microstate C is generally the most dominant state during eyes-closed rest (57, 125). Recently, Seitzman et al. (126) showed that microstate C decreases in duration and occurrence during a mental arithmetic task, similar to our findings. Decrease of microstate C

duration has also been described when subjects are engaged in object or verbal visualization tasks compared to rest (127). Based on these and other studies, it is assumed that microstate C reflects activity in the DMN (91, 126, 127). For a discussion, see (54). Indeed, our analysis of the sources underlying this microstate confirms such interpretation. The sources of microstate C were located bilaterally in the lateral part of the parietal lobe and MTG, areas that we attributed to "self-experience subsystem" of the DMN. The observation that microstate C is not significantly boosted by the memory condition compared to rest is not surprising. It confirms the assumption that self-relevant memory retrieval also predominates during spontaneous mind wandering, hence the sub-system of the DMN including the lateral areas of the parietal lobe is strongly active.

Moreover, our investigation revealed that microstate B increased in occurrence during the memory as compared to both rest and math conditions. This state has been previously attributed to the visual network (60, 91, 128). For example, Milz et al. (127) showed that microstate B increased when participants were asked to visualize previously presented images. Source localization in our study also indicated strong activation of the visual cortex together with medial parietal areas. Intriguingly, lesions to the medial parietal cortex cause memory recognition and visuospatial impairments, but no impairments related to self-consciousness (129). We thus interpret the increased occurrence of microstate B as related to the "scene-construction subsystem" found in the fMRI connectivity analysis, while microstate C is related to the "self-experience subsystem", which becomes active when reflecting on one's subjective mental states. An intriguing assumption is therefore that the microstate analysis allows us to disentangle the sub-parts of thoughts related to the conscious experience of an episodic autobiographic memory, i.e. visualization of the scene and visualization of the self in the scene. Indeed, the transition probability analysis revealed a more frequent switching between microstate B and C than between any other state.

Additionally, our results show that while both microstates B and C are less frequently appearing when participants are engaged in math calculations, microstate D strongly increases in duration and occurrence during this condition. Microstate D has previously been attributed to the attention/cognitive control network including frontoparietal areas (60, 91, 128) and our source localization of microstate D confirmed the attribution of this state to the frontoparietal control network (FPCN) (65, 89, 98, 99). Furthermore, the observation of increase of microstate D and decrease of microstate C fits very well to the observation that the FPCN and the DMN are inversely activated when participants are engaged in external-directed and self-directed cognition

(79, 89, 89, 130, 131). Therefore, we show that the large-scale network anti-correlation found in the fMRI data is associated with sub-second modulation of the presence of microstates sub-serving these functions.

In conclusion, our results provide new insights on the neuronal signature of fMRI resting-state networks: increased BOLD activity is due to longer lasting and more frequently re-occurring periods of neuronal synchronization within the network in the sub-second scale. By combining fMRI and EEG, we provide direct evidence of capturing and enhancing the spatial and temporal dynamics of specific self-related and self-unrelated thoughts. Particularly, the fMRI connectivity results revealed two memory subsystems, the "self-experience" and "scene-construction" networks with distinct functional and anatomical characteristics. The EEG microstate analysis showed that states can be selectively enhanced by instructing participants, and these states then appear more often and last longer. Using EEG source-imaging we show that the networks underlying these microstates are strikingly similar to those showing significantly increased BOLD activity and connectivity when participants perform the same instructed-thought task in the MRI scanner. This result provides direct evidence that the RSNs captured by fMRI are tightly linked to, and possibly originated by, a prolongation and repeated occurrence of states of synchronized activity of specific large-scale neuronal networks, in the sub-second timescale.

Materials and Methods

Participants and Experimental Paradigm

We included 15 healthy participants (30.5±5.5years, 5 male/10 female) in this study. The work was approved by the institutional review board of the local ethics committee, and all participants provided written informed consent prior to the experiment. Each participant underwent three sessions: i. an interview session, ii. an EEG recording session, and iii. an fMRI session. During the interview, all participants performed a classical autobiographical memory questionnaire (ABMQ) (132) in order to select vividly remembered images, which were then used for the EEG and fMRI sessions. We used high-density 64-channel EEG and 7T-fMRI recordings in three distinct conditions (Fig. 1): eyes-closed rest – termed "rest condition" (6min), mentally retrieving personal past episodes – termed "memory condition" (10min), and mental arithmetic operations – termed "math condition" (10min). The memory and math conditions comprised twenty 30-s trials each. On each trial, a personal image (e.g., photo of a participant with a birthday cake) or a calculation (e.g., 447-7=) was presented for 5sec, followed by a 20sec period of closed-eyes during which the participants retrieved the past event or continued to serially subtract/add the given number. After this period, there was a question: *"How much did you relive the original event?"*

for the memory task and *"How much attention did you pay to the calculation?"* for the mental arithmetic task. The time allowed to read and respond to the question was 5sec. Participants answered by a button press (1 =not at all to 4=fully). These ratings allowed us to control for an active involvement of our participants in the study. Room lights were switched off during both fMRI and EEG acquisitions. The ratings were comparable between the EEG (M=3.2, SEM=0.12) and the fMRI (M=3.1, SEM=0.11) memory session as well as the EEG (M=3.5, SEM=0.12) and the fMRI (M=3.41, SEM=0.11) math session.

fMRI Acquisition

The fMRI sessions were conducted on an actively shielded Magnetom 7T head scanner (Siemens, Erlangen, Germany), equipped with AC84 head gradients (80mT/m max. gradient strength, 333 T/m/s max. slew-rate) and an 8-channel transmit/receive head loop array (Rapid Biomedical, Rimpar, Germany). During each paradigm, whole-brain functional data were acquired using a simultaneous multi-slice (SMS) 2D GE-EPI sequence, with TR/TE = 1000/22ms, α = 54°, 110×110 matrix size with 2.0 mm isotropic spatial resolution, 75 sagittal slices with 3× SMS acceleration and 1/3 field-of-view (FOV) CAIPI shift (133), 2× in-plane GRAPPA acceleration (anterior-posterior direction) and 7/8 partial Fourier undersampling. This protocol was designed to simultaneously provide fairly high temporal resolution (1 volume/s) and spatial resolution (2-mm voxel width), with whole-brain coverage. For each subject, an additional 5-volume scan was also performed with reversed phase encoding direction (posterior-anterior), for subsequent correction of susceptibility-induced EPI distortions. To aid spatial co-registration, T_1-weighted anatomical data were acquired with a 3D MP2RAGE sequence (134) with $TR/TI_1/TI_2/TE$ = 5500/750/2350/1.87 ms and 1 mm isotropic spatial resolution.

fMRI Pre-processing

The fMRI data were processed using the FMRIB Software Library (FSL v5.0, Oxford, UK) combined with Matlab routines developed in-house (Mathworks, Natick MA, USA). Data pre-processing included motion correction (MCFLIRT tool, 6 degrees of freedom) (135), slice-timing adjustment (set to the middle of each TR, via linear interpolation), brain segmentation (BET tool) (136), Gaussian spatial smoothing (FWHM = 4mm) and temporal de-trending (100sec cut off). To reduce contributions from head motion, a set of 24 confound regressors derived from the motion parameter time courses were regressed out of the fMRI data by general linear model analysis. Each dataset was co-registered to the standard MNI space as follows: first, for each subject, the fMRI data were B_0-unwarped using FSL-TOPUP (137) and brought to the

subject's anatomical space using FLIRT with boundary-based registration (138) (12 degrees of freedom). The co-registration to MNI space was then determined using the anatomical images, again through FLIRT (12 degrees of freedom).

Fractional Amplitude of Low Frequency Fluctuations (fALFF) Analysis

Voxel-wise fALFF values were estimated for the pre-processed fMRI data of each subject and paradigm, in native space, as proposed by Zou et al. (70): the time series of each voxel was transformed to the frequency domain and the sum of amplitudes in the 0.01–0.08 Hz interval was divided by the sum of amplitudes of the full frequency band. The individual fALFF maps thus obtained for each paradigm and subject were then brought to MNI space for group analysis. The fALFF maps were compared between the memory and maths conditions using paired T-tests across subjects, and statistical significance was determined using topological false-discovery rate (FDR) inference to correct for multiple comparisons (72) (cluster-forming threshold $T > 2.20$, FDR $\alpha = 5\%$).

Functional Connectivity Analysis

The brain regions (clusters) displaying significant fALFF changes between the memory and maths conditions were further considered for connectivity analysis. These regions were warped to each individual run's native space, and the voxels belonging to each region were identified. The functional connectivity between each pair of regions was estimated as the average Pearson correlation value between the time course of every voxel in the first region with that of every voxel in the second region. The estimations were organized in a connectivity matrix, and also included an estimation for each region paired with itself, serving as a measure of functional homogeneity within the region.

EEG Acquisition and Pre-Processing

EEG was recorded with a 64-channel Brain Amp EEG system (Brain Products, Munich, Germany). Offline, the EEG was down-sampled to 250Hz, bad electrodes were interpolated using a 3-D spherical spline, band-pass filtered between 1-40Hz (Butterworth filter of 2nd order) and re-computed to the common average-reference. Infomax-based Independent Component Analysis (ICA) was applied to remove oculomotor and cardiac artefacts based on the channels with maximal amplitude, the topography, and time course of the ICA component.

Microstate Analysis

K-means clustering

The free academic software Cartool was used for the microstate analysis (139). It uses a modified k-means cluster analysis (140) to determine the most dominant scalp potential maps in each individual subject ignoring polarity. Only maps at local maxima of the Global Field Power (GFP) enter the cluster analysis as they represent time points of highest signal-to-noise ratio (141). The optimal number of cluster maps was determined individually for each subject using a meta-criterion consisting of seven different criteria described in the literature (*SI Appendix,* SMethod1). The number of optimal clusters varied between 4 and 8. A second k-means cluster analysis was then applied on these individual cluster maps to determine the most dominant maps across subjects for each condition, again using the meta-criterion to determine the optimal number of maps. This second clustering resulted in 6 cluster maps for each condition.

Back-fitting

The six group cluster maps of a given condition were fitted back to the original EEG of each subject, including all data points except for periods that were marked as artefacts. Back-fitting means that the spatial correlation between the six cluster maps and each individual data point was calculated and the data point was labelled with the cluster map that showed the highest correlation (winner takes all, see e.g. (55, 60)). Note that the polarity of the maps was again ignored in this back-fitting procedure. Data points where none of the six maps reached a correlation higher than 50% were labelled as "non-assigned". Once the whole recording was labelled, a temporal smoothing was applied by ignoring segments where a given cluster map was present for less than 4 time points (32ms) and the time points were split and assigned to the preceding and following cluster map. Two temporal parameters were then quantified for each recording of each subject: the mean duration of the continued presence of a given map, and the number of times per second a given microstate appeared, independent of the duration – termed "occurrence" (Figs. 3c and 3d). To investigate differences between conditions and microstates we performed repeated measure ANOVAs with the factors "condition" (rest, math, memory) for each microstate class. We applied a threshold of $p<.0001$ to correct for multiple testing and performed post-hoc comparisons only if this threshold was reached.

Source Localization

In order to estimate the sources contributing to each of the six microstates we calculated a distributed linear inverse solution (LAURA). The lead field for the inverse solution was calculated for 64 electrode positions and the average brain of the Montreal Neurological Institute

in a grey matter constrained head model using a modified version of the SMAC (142) head model (LSMAC) with 5000 distributed solution points (139). All time points that were attributed to a given microstate were concatenated for each subject and source localization was applied to each of these time points. Normalization across time was done for each solution point in order to eliminate activation biases (*SI Appendix,* SMethod2). The estimated current densities were then averaged across time points for each solution point and each subject in each condition (*SI Appendix,* SFigs. 2-4).

Analysis of transition probabilities

We analyzed the syntax of EEG microstates by computing the probabilities from a single n^{th}-previous state to the current one for each subject and transition pair and normalized it by all between-class transitions (125, 143). In order to account for the variability of occurrence of the microstates we divided the observed probability by the expected probability if the state transitions occurred randomly, i.e. are proportional to the relative occurrence of the state. The expected probability is calculated as $P(x \rightarrow y) = PxPy/(1-Px)$, where Px and Py are the relative occurrence of microstate X and Y, i.e., the number of occurrences divided by the total number of microstates observed (143). The so-derived transition probabilities were then compared between all possible transitions into the current one and from the current one into all other ones.

References:

1. Kucyi A (2017) Just a thought: How mind-wandering is represented in dynamic brain connectivity. *Neuroimage* 1–10.
2. Christoff K (2012) Undirected thought: Neural determinants and correlates. *Brain Res* 1428:51–59.
3. Fox KCR, Spreng RN, Ellamil M, Andrews-Hanna JR, Christoff K (2015) The wandering brain: Meta-analysis of functional neuroimaging studies of mind-wandering and related spontaneous thought processes. *Neuroimage* 111:611–621.
4. Fox MD, Raichle ME (2007) Spontaneous fluctuations in brain activity observed with functional magnetic resonance imaging. *Nat Rev Neurosci* 8(9):700–711.
5. Raichle ME (2015) The Brain's Default Mode Network. *Annu Rev Neurosci* 38(1):433–447.
6. Greicius MD, Krasnow B, Reiss AL, Menon V (2003) Functional connectivity in the resting brain: a network analysis of the default mode hypothesis. *Proc Natl Acad Sci U S A* 100(1):253–8.
7. Smith SM, et al. (2009) Correspondence of the brain's functional architecture during activation and rest. *Proc Natl Acad Sci* 106(31):13040–13045.
8. Andrews-Hanna JR, Reidler JS, Huang C, Buckner RL (2010) Evidence for the Default Network's Role in Spontaneous Cognition. *J Neurophysiol* 104(1):322–335.
9. Kucyi A, Salomons T V, Davis KD (2013) Mind wandering away from pain dynamically engages antinociceptive and default mode brain networks. *PNAS* 110(46):18692–18697.
10. Fox KCR, Ph D, Christoff K, Editors PD, Fox KCR (2018) *The Oxford Handbook of Spontaneous Thought.*
11. Smallwood J, Schooler JW (2015) The Science of Mind Wandering: Empirically

Navigating the Stream of Consciousness. *Annu Rev Psychol* 66(1):487–518.
12. Kucyi A, Esterman M, Riley CS, Valera EM (2016) Spontaneous default network activity reflects behavioral variability independent of mind-wandering. *Proc Natl Acad Sci* 113(48):13899–13904.
13. Stawarczyk D, Majerus S, Maquet P, D'Argembeau A (2011) Neural correlates of ongoing conscious experience: Both task-unrelatedness and stimulus-independence are related to default network activity. *PLoS One* 6(2).
14. Perogamvros L, et al. (2017) The phenomenal contents adn neural correlates of spontaneous thoughts across wakefulness, NREM sleep, and REM sleep. *J Cogn Neurosci* 29(10):1766–1777.
15. Lehmann D, Strik WK, Henggeler B, Koenig T, Koukkou M (1998) Brain electric microstates and momentary conscious mind states as building blocks of spontaneous thinking : I . Visual imagery and abstract thoughts. *Int J Psychophysiol* 29:1–11.
16. Vanhaudenhuyse A, et al. (2011) Two Distinct Neuronal Networks Mediate the Awareness of Environment and of Self. *J Cogn Neurosci* 23(3):570–578.
17. Dixon ML, et al. (2017) Interactions between the default network and dorsal attention network vary across default subsystems, time, and cognitive states. *Neuroimage* 147:632–649.
18. Christoff K, Gordon AM, Smallwood J, Smith R, Schooler JW (2009) Experience sampling during fMRI reveals default network and executive system contributions to mind wandering. *Proc Natl Acad Sci* 106(21):8719–8724.
19. Ellamil M, et al. (2016) Dynamics of neural recruitment surrounding the spontaneous arising of thoughts in experienced mindfulness practitioners. *Neuroimage* 136:186–196.
20. Andrews-Hanna JR, Reidler JS, Sepulcre J, Poulin R, Buckner RL (2010) Functional-Anatomic Fractionation of the Brain's Default Network. *Neuron* 65(4):550–562.
21. Axelrod V, Rees G, Bar M (2017) The default network and the combination of cognitive processes that mediate self-generated thought. *Nat Hum Behav* 1(12):896–910.
22. Shirer WR, Ryali S, Rykhlevskaia E, Menon V, Greicius MD (2012) Decoding subject-driven cognitive states with whole-brain connectivity patterns. *Cereb Cortex* 22(1):158–165.
23. Delamillieure P, et al. (2010) The resting state questionnaire: An introspective questionnaire for evaluation of inner experience during the conscious resting state. *Brain Res Bull* 81(6):565–573.
24. Biswal BB, Kylen J Van, Hyde JS (1997) Simultaneous assessment of flow and BOLD signals in resting-state functional connectivity maps. *NMR Biomed* 10(4–5):165–170.
25. Biswal BB, et al. (2010) Toward discovery science of human brain function. *Proc Natl Acad Sci* 107(10):4734–4739.
26. Buckner RL (2012) The serendipitous discovery of the brain's default network. *Neuroimage* 62(2):1137–1145.
27. Power JD, et al. (2011) Functional Network Organization of the Human Brain. *Neuron* 72(4):665–678.
28. Christoff K, Irving ZC, Fox KCR, Spreng RN, Andrews-Hanna JR (2016) Mind-wandering as spontaneous thought: A dynamic framework. *Nat Rev Neurosci* 17(11):718–731.
29. Bressler SL, Menon V (2010) Large-scale brain networks in cognition: emerging methods and principles. *Trends Cogn Sci* 14(6):277–290.
30. Davis SW, Stanley ML, Moscovitch M, Cabeza R (2017) Resting-state networks do not determine cognitive function networks: a commentary on Campbell and Schacter (2016). *Lang Cogn Neurosci* 32(6):669–673.
31. Spreng RN, Schacter DL (2012) Default Network Modulation and Large-Scale Network Interactivity in Healthy Young and Old Adults. *Cereb Cortex* 22(11):2610–2621.
32. Shulman GL, et al. (1997) Common Blood Flow Changes across Visual Tasks: II.

Decreases in Cerebral Cortex. *J Cogn Neurosci* 9(5):648–663.
33. Raichle ME, et al. (2001) A default mode of brain function. *Proc Natl Acad Sci U S A* 98(2):676–682.
34. Spreng RN, Mar R a, Kim ASN (2009) The common neural basis of autobiographical memory, prospection, navigation, theory of mind, and the default mode: a quantitative meta-analysis. *J Cogn Neurosci* 21(3):489–510.
35. Peer M, Salomon R, Goldberg I, Blanke O, Arzy S (2015) Brain system for mental orientation in space, time, and person. *Proc Natl Acad Sci* 112(35):11072–11077.
36. Hassabis D, et al. (2014) Imagine All the People: How the Brain Creates and Uses Personality Models to Predict Behavior. *Cereb Cortex* 24(8):1979–1987.
37. Cabral J, Kringelbach ML, Deco G (2017) Functional connectivity dynamically evolves on multiple time-scales over a static structural connectome: Models and mechanisms. *Neuroimage* 160:84–96.
38. Vidaurre D, Smith SM, Woolrich MW (2017) Brain network dynamics are hierarchically organized in time. *Proc Natl Acad Sci* 114 (48) 12827-12832.
39. Karahanoğlu FI, Van De Ville D (2015) Transient brain activity disentangles fMRI resting-state dynamics in terms of spatially and temporally overlapping networks. *Nat Commun* 6:7751.
40. Zalesky A, Fornito A, Cocchi L, Gollo LL, Breakspear M (2014) Time-resolved resting-state brain networks. *Proc Natl Acad Sci* 111(28):10341–10346.
41. de Pasquale F, Corbetta M, Betti V, Della Penna S (2017) Cortical cores in network dynamics. *Neuroimage*. doi:10.1016/j.neuroimage.2017.09.063.
42. Hutchinson JB, et al. (2014) Functional heterogeneity in posterior parietal cortex across attention and episodic memory retrieval. *Cereb Cortex* 24(1):49–66.
43. Power JD, Schlaggar BL, Petersen SE (2014) Studying brain organization via spontaneous fMRI signal. *Neuron* 84(4):681–696.
44. Cole MW, et al. (2013) Multi-task connectivity reveals flexible hubs for adaptive task control. *Nat Neurosci* 16(9):1348–1355.
45. Cole MW, Bassett DS, Power JD, Braver TS, Petersen SE (2014) Intrinsic and task-evoked network architectures of the human brain. *Neuron* 83(1):238–251.
46. James W (1890) *The Principles of Psychology*.
47. Efron R (1970) The Minimum Duration of a perception. *Neuropsychologia* 8:57–63.
48. Baars BJ (1997) In the Theater of Consciousness:The Workspace of the Mind. *Oxford Oxford Univ Press*.
49. Dehaene S, Kerszberg M, Changeux J-P (1998) A neuronal model of a global workspace in effortful cognitive tasks. *Proc Natl Acad Sci* 95(24):14529–14534.
50. Rabinovich M, et al. (2001) Dynamical encoding by networks of competing neuron groups: Winnerless competition. *Phys Rev Lett* 87(6):681021–681024.
51. Huys R, Perdikis D, Jirsa VK (2014) Functional architectures and structured flows on manifolds: A dynamical framework for motor behavior. *Psychol Rev* 121(3):302–336.
52. Meehan TP, Bressler SL (2012) Neurocognitive networks: Findings, models, and theory. *Neurosci Biobehav Rev* 36(10):2232–2247.
53. Deco G, Jirsa VK, McIntosh AR (2011) Emerging concepts for the dynamical organization of resting-state activity in the brain. *Nat Rev Neurosci* 12(1):43–56.
54. Michel CM, Koenig T (2018) EEG microstates as a tool for studying the temporal dynamics of whole-brain neuronal networks: A review. *Neuroimage* 1–17.
55. Van De Ville D, Britz J, Michel CM (2010) EEG microstate sequences in healthy humans at rest reveal scale-free dynamics. *Proc Natl Acad Sci* 107(42):18179–18184.
56. Khanna A, Pascual-leone A, Michel CM, Farzan F (2015) Neuroscience and Biobehavioral Reviews Microstates in resting-state EEG : Current status and future directions. *Neurosci Biobehav Rev* 49:105–113.

57. Koenig T, et al. (2002) Millisecond by Millisecond , Year by Year : Normative EEG Microstates and Developmental Stages. 48:41–48.
58. Changeux JP, Michel CM (2004) Mechanisms of neural integration at the brain-scale level. The neuronal workspace and microstate models. *Microcircuits Interface Between Neurons Glob Brain Funct* 347–370.
59. Baars BBJ (2002) Atoms of thought. *Brain* (3):1–4.
60. Britz J, Van De Ville D, Michel CM (2010) BOLD correlates of EEG topography reveal rapid resting-state network dynamics. *Neuroimage* 52(4):1162–1170.
61. Mantini D, Perrucci MG, Gratta C Del, Romani GL, Corbetta M (2007) Electrophysiological signatures of resting state networks in the human brain. *Proc Natl Acad Sci USA* 104(32):13170–13175.
62. Musso F, Brinkmeyer J, Mobascher A, Warbrick T, Winterer G (2010) Spontaneous brain activity and EEG microstates. A novel EEG/fMRI analysis approach to explore resting-state networks. *Neuroimage* 52(4):1149–1161.
63. Yuan H, Zotev V, Phillips R, Drevets WC, Bodurka J (2012) Spatiotemporal dynamics of the brain at rest - Exploring EEG microstates as electrophysiological signatures of BOLD resting state networks. *Neuroimage* 60(4):2062–2072.
64. Corbetta M, Shulman GL (2002) Control of goal-directed and stimulus-driven attention in the brain. *Nat Rev Neurosci* 3(3):201–215.
65. Sestieri C, Shulman GL, Corbetta M (2017) The contribution of the human posterior parietal cortex to episodic memory. *Nat Rev Neurosci* 18(3):183–192.
66. Foster BL, Parvizi J (2012) Resting oscillations and cross-frequency coupling in the human posteromedial cortex. *Neuroimage* 60(1):384–391.
67. Foster BL, Rangarajan V, Shirer WR, Parvizi J (2015) Intrinsic and task-dependent coupling of neuronal population activity in human parietal cortex. *Neuron* 86(2):578–590.
68. Fox KCR, Foster BL, Kucyi A, Daitch AL, Parvizi J (2018) Intracranial Electrophysiology of the Human Default Network. *Trends Cogn Sci* 22(4):307–324.
69. Parvizi J, Wagner AD (2018) Memory, Numbers, and Action Decision in Human Posterior Parietal Cortex. *Neuron* 97(1):7–10.
70. Zou QH, et al. (2008) An improved approach to detection of amplitude of low-frequency fluctuation (ALFF) for resting-state fMRI: Fractional ALFF. *J Neurosci Methods* 172(1):137–141.
71. Biswal BB (2012) Resting state fMRI: A personal history. *Neuroimage* 62(2):938–944.
72. Chumbley J, Worsley K, Flandin G, Friston K (2010) Topological FDR for neuroimaging. *Neuroimage* 49(4):3057–3064.
73. Svoboda E, Mckinnon MC, Levine B (2006) The functional neuroanatomy of autobiographical memory : A meta-analysis. *Neuropsychologia* 44:2189–2208.
74. Kim H (2016) Default network activation during episodic and semantic memory retrieval: A selective meta-analytic comparison. *Neuropsychologia* 80:35–46.
75. Martinelli P, Sperduti M, Piolino P (2013) Neural Substrates of the Self-Memory System : New Insights from a Meta-Analysis. *Hum Brain Mapp* 1529(34):1515–1529.
76. Spreng RN, Grady CL (2009) Patterns of Brain Activity Supporting Autobiographical Memory, Prospection, and Theory of Mind, and Their Relationship to the Default Mode Network. *J Cogn Neurosci* 22(6):1112–1123.
77. Schacter DL, et al. (2012) The Future of Memory : Remembering, Imagining and the Brain. *Neuron Rev* 76:677–694.
78. Sestieri C, Corbetta M, Romani GL, Shulman GL (2011) Episodic memory retrieval, parietal cortex, and the default mode network: functional and topographic analyses. *J Neurosci* 31(12):4407–20.
79. Spreng NR, Madore KP, Schacter DL (2018) Better imagined: Neural correlates of the episodic simulation boost to prospective memory performance. *Neuropsychologia*.

doi:10.1016/j.neuropsychologia.2018.03.025.
80. Fehr T, Code C, Herrmann M (2007) Common brain regions underlying different arithmetic operations as revealed by conjunct fMRI-BOLD activation. *Brain Res* 1172(1):93–102.
81. Amalric M, Dehaene S (2016) Origins of the brain networks for advanced mathematics in expert mathematicians. *Proc Natl Acad Sci* 113(18):4909–4917.
82. Arsalidou M, Taylor MJ (2011) Is 2+2=4? Meta-analyses of brain areas needed for numbers and calculations. *Neuroimage* 54(3):2382–2393.
83. Hamid AIA, Yusoff AN, Mukari SZMS, Mohamad M (2011) Brain activation during addition and subtraction tasks in-noise and in-quiet. *Malaysian J Med Sci* 18(2):3–15.
84. Nieder A, Dehaene S (2009) Representation of Number in the Brain. *Annu Rev Neurosci* 32(1):185–208.
85. Dastjerdi M, Ozker M, Foster BL, Rangarajan V, Parvizi J (2013) Numerical processing in the human parietal cortex during experimental and natural conditions. *Nat Commun* 4:1–11.
86. Foster BL, Dastjerdi M, Parvizi J (2012) Neural populations in human posteromedial cortex display opposing responses during memory and numerical processing. *Proc Natl Acad Sci* 109(38):15514–15519.
87. Andrews-Hanna JR, Saxe R, Yarkoni T (2014) Contributions of episodic retrieval and mentalizing to autobiographical thought: evidence from functional neuroimaging, resting-state connectivity, and fMRI meta-analyses. *Neuroimage* 91:324–35.
88. Sestieri C, Corbetta M, Romani GL, Shulman GL (2011) Episodic Memory Retrieval, Parietal Cortex, and the Default Mode Network: Functional and Topographic Analyses. *J Neurosci* 31(12):4407–4420.
89. Dixon ML, et al. (2018) Heterogeneity within the frontoparietal control network and its relationship to the default and dorsal attention networks. *Proc Natl Acad Sci* 115(7):E1598–E1607.
90. Grieder M, et al. (2016) Clinical Neurophysiology Discovering EEG resting state alterations of semantic dementia. *Clin Neurophysiol* 127(5):2175–2181.
91. Custo A, van der Ville D, Wells WM, Tomescu IM, Michel C (2017) EEG Resting-State Networks: microstates' source localization. *Brain Connect* XX(Xx):brain.2016.0476.
92. Grave De Peralta Menendez R, Murray MM, Michel CM, Martuzzi R, Gonzalez Andino SL (2004) Electrical neuroimaging based on biophysical constraints. *Neuroimage* 21(2):527–539.
93. Pascual-Marqui RD, et al. (2014) The resting microstate networks (RMN): cortical distributions, dynamics, and frequency specific information flow. 1–14.
94. Simons JS, Peers P V., Mazuz YS, Berryhill ME, Olson IR (2010) Dissociation between memory accuracy and memory confidence following bilateral parietal lesions. *Cereb Cortex* 20(2):479–485.
95. Staresina BP, Alink A, Kriegeskorte N, Henson RN (2013) Awake reactivation predicts memory in humans. *Proc Natl Acad Sci* 110(52):21159–21164.
96. Davachi L, Mitchell JP, Wagner AD (2003) Multiple routes to memory: Distinct medial temporal lobe processes build item and source memories. *Proc Natl Acad Sci* 100(4):2157–2162.
97. Staresina BP, Duncan KD, Davachi L (2011) Perirhinal and Parahippocampal Cortices Differentially Contribute to Later Recollection of Object- and Scene-Related Event Details. *J Neurosci* 31(24):8739–8747.
98. Ptak R, Schnider A, Fellrath J (2017) The Dorsal Frontoparietal Network: A Core System for Emulated Action. *Trends Cogn Sci* 21(8):589–599.
99. Boly M, et al. (2017) Are the Neural Correlates of Consciousness in the Front or in the Back of the Cerebral Cortex? Clinical and Neuroimaging Evidence. *J Neurosci*

37(40):9603–9613.
100. Koch C (2018) What is consciousness? *Nature* 557:9–11.
101. Scoviille WB (1957) Loss of recent memory after bilateral hippocampal lesions. *J Neurol Neurosurg Psychiatry*.
102. Steinvorth S, Levine B, Corkin S (2005) Medial temporal lobe structures are needed to re-experience remote autobiographical memories: Evidence from H.M. and W.R. *Neuropsychologia* 43(4):479–496.
103. Cabeza R, St Jacques P (2007) Functional neuroimaging of autobiographical memory. *Trends Cogn Sci* 11(5):219–27.
104. Daselaar SM, et al. (2008) The spatiotemporal dynamics of autobiographical memory: neural correlates of recall, emotional intensity, and reliving. *Cereb cortex* 18(1):217–29.
105. Clark IA, Maguire EA (2016) Remembering Preservation in Hippocampal Amnesia. *Annu Rev Psychol* 67(1):51–82.
106. St Jacques PL, Olm C, Schacter DL (2013) Neural mechanisms of reactivation-induced updating that enhance and distort memory. *PNAS* 110(49):19671–8.
107. Zeidman P, Maguire EA (2016) Anterior hippocampus: The anatomy of perception, imagination and episodic memory. *Nat Rev Neurosci* 17(3):173–182.
108. Corkin S (2002) What's new with the amnesic patient H. M.? *Nat Rev Neurosci* 3(February):153–160.
109. Damasio A, Damasio H, Tranel D (2013) Persistence of feelings and sentience after bilateral damage of the insula. *Cereb Cortex* 23(4):833–846.
110. Ben-Zvi S, Soroker N, Levy DA (2015) Parietal lesion effects on cued recall following pair associate learning. *Neuropsychologia* 73:176–194.
111. Berryhill ME, Phuong L, Picasso L, Cabeza R, Olson IR (2007) Parietal Lobe and Episodic Memory: Bilateral Damage Causes Impaired Free Recall of Autobiographical Memory. *J Neurosci* 27(52):14415–14423.
112. Hower KH, Wixted J, Berryhill ME, Olson IR (2014) Impaired perception of mnemonic oldness, but not mnemonic newness, after parietal lobe damage. *Neuropsychologia* 56(1):409–417.
113. Rugg MD, King DR (2017) Ventral lateral parietal cortex and episodic memory retrieval. *Cortex*:1–13.
114. Tononi G, Boly M, Massimini M, Koch C (2016) Integrated information theory: From consciousness to its physical substrate. *Nat Rev Neurosci* 17(7):450–461.
115. Corbetta M, Shulman GL (2011) *Spatial Neglect and Attention Networks* doi:10.1146/annurev-neuro-061010-113731.
116. Bréchet L, Mange R, Herbelin B, Gauthier B, Blanke O (2018) Viewing one ' s body during encoding boosts episodic memory.
117. Tulving E (1985) Memory and consciousness. Cnadadian Psychology 26 (1): 1-12.
118. Tulving E (2005) Episodic memory and autonoesis: Uniquely human? In H. S. Terrace, & J. Metcalfe (Eds.), The Missing Link in Cognition (pp. 4-56). NewYork, NY: Oxford University Press. *Cognition* 4–56.
119. Koch C, Massimini M, Boly M, Tononi G (2016) Neural correlates of consciousness: Progress and problems. *Nat Rev Neurosci* 17(5):307–321.
120. Dehaene S, et al. (2017) What is consciousness, and could machines have it? *Science (80-)* 358(6362):484–489.
121. Bréchet L, Grivaz P, Gauthier B, Blanke O Common recruitment of angular gyrus in episodic autobiographical memory and bodily self-consciousness. 1–18.
122. Dehaene S, Changeux JP (2011) Experimental and Theoretical Approaches to Conscious Processing. *Neuron* 70(2):200–227.
123. Seth AK, Baars BJ (2005) Neural Darwinism and consciousness. *Conscious Cogn* 14(1):140–168.

124. Khanna A, Pascual-leone A, Farzan F (2014) Reliability of Resting-State Microstate Features in Electroencephalography. 1–21.
125. Tomescu MI, et al. (2018) From swing to cane: Sex differences of EEG resting-state temporal patterns during maturation and aging. *Dev Cogn Neurosci* 31:58–66.
126. Seitzman BA, et al. (2016) Cognitive manipulation of brain electric microstates. NeuroImage doi:10.1016/j.neuroimage.2016.10.002.
127. Milz P, et al. (2016) The functional significance of EEG microstates-Associations with modalities of thinking. *Neuroimage* 125:643–656.
128. Custo A, Vulliemoz S, Grouiller F, Van De Ville D, Michel C (2014) EEG source imaging of brain states using spatiotemporal regression. *Neuroimage* 96:106–116.
129. Davidson PSR, et al. (2010) from Focal Lesion Patients. 46(7):1743–1755.
130. Spreng RN, Sepulcre J, Turner GR, Stevens WD, Schacter DL (2013) Intrinsic Architecture Underlying the Relations among the Default, Dorsal Attention, and Frontoparietal Control Networks of the Human Brain. *J Cogn Neurosci* 25(1):74–86.
131. Fox MD, et al. (2005) From The Cover: The human brain is intrinsically organized into dynamic, anticorrelated functional networks. *Proc Natl Acad Sci* 102(27):9673–9678.
132. Rubin DC, Schrauf RW, Greenberg DL (2003) Belief and recollection of autobiographical memories. *Mem Cognit* 31(6):887–901.
133. Setsompop K, et al. (2012) Blipped-controlled aliasing in parallel imaging for simultaneous multislice echo planar imaging with reduced g-factor penalty. *Magn Reson Med* 67(5):1210–1224.
134. Marques JP, et al. (2010) MP2RAGE, a self bias-field corrected sequence for improved segmentation and T1-mapping at high field. *Neuroimage* 49(2):1271–1281.
135. Jenkinson M, Bannister P, Brady M, Smith S (2002) Improved Optimization for the Robust and Accurate Linear Registration and Motion Correction of Brain Images Improved Optimization for the Robust and Accurate Linear Registration and Motion Correction of Brain Images. *Neuroimage* 17:825–841.
136. Smith SM (2002) Fast robust automated brain extraction. *Hum Brain Mapp* 17(3):143–155.
137. Andersson JLR, Skare S, Ashburner J (2003) How to correct susceptibility distortions in spin-echo echo-planar images: Application to diffusion tensor imaging. *Neuroimage* 20(2):870–888.
138. Greve DN, Fischl B (2009) Accurate and robust brain image alignment using boundary-based registration. *Neuroimage* 48(1):63–72.
139. Brunet D, Murray MM, Michel CM (2011) Spatiotemporal analysis of multichannel EEG: CARTOOL. *Comput Intell Neurosci* 2011. doi:10.1155/2011/813870.
140. Pascual-Marqui RD, Michel CMM, Lehmann D (1994) Low resolution electromagnetic tomography: a new method for localizing electrical activity in the brain. *Int J Psychophysiol* 18(1):49–65.
141. Koenig T, Brandeis D (2016) NeuroImage Inappropriate assumptions about EEG state changes and their impact on the quanti fi cation of EEG state dynamics. *Neuroimage* 125:1104–1106.
142. Spinelli L, Andino SG, Lantz G, Seeck M, Michel CM (2000) Electromagnetic Inverse Solutions in Anatomically Constrained Spherical Head Models. *Brain Topogr* 13(2):115–125.
143. Lehmann D, et al. (2005) EEG microstate duration and syntax in acute , medication-na R ve , first-episode schizophrenia : a multi-center study. *Psychiatry Res Neuroimaging* 138:141–156.

Supplementary Method 1: Criteria for evaluating the optimal number of microstate maps

7 criteria have been used to evaluate independently the quality of each clustering. They were then merged together in order to derive a single synthetic meta-criterion. This improves the confidence in the right estimation of the optimal number of clusters, as compared to previous work relying on single criterion only (i.e. Cross-Validation criterion (1) or the Krzanowski-Lai Index (2)).

The following 7 criteria were taken from (1, 3–5):

Gamma: An adaptation of Goodman and Kruskal, based on concordant *vs.* discordant clustered pairs.

Silhouettes: Evaluation of the consistency of each cluster through its goodness of fit.

Davies and Bouldin: A function of the sum of the ratio of within-cluster to between-cluster separation.

Point-Biserial: A point-biserial correlation calculated between the distance matrix and a binary cluster index.

Dunn: An evaluation of the goodness of separation of all clusters.

Krzanowski-Lai Index: A ratio of the relative difference of the within clusters dispersion.

Cross-Validation: A modified version of the predictive residual variance.

The meta-criterion is defined as the median of all optimal number of clusters across all criteria (*Supplementary Figures,* Fig. S5). The meta-criterion calculation is implemented in the free academic software Cartool (https://sites.google.com/site/cartoolcommunity/). Note that this is an improved method of the earlier version that was used in

References:

1. Pascual-Marqui RD, Michel CM, Lehmann D (1995) Segmentation of brain electrical activity into microstates: model estimation and validation. *IEEE Trans* 42(7):1–24.
2. Murray MM, Brunet D, Michel CM (2008) Topographic ERP analyses: A step-by-step tutorial review. *Brain Topogr* 20(4):249–264.
3. Charrad M, Ghazzali N, Boiteau V, Niknafs A (2014) NbClust : An R Package for Determining the. *J Stat Softw* 61(6):1–36.
4. Krzanowski WJ, Lai YT (1988) A Criterion for Determining the Number of Groups in a Data Set Using Sum-of-Squares Clustering. *Biometrics* 44(1):23–34.
5. Milligan GW, M. C.Cooper (1985) An examination of procedures for determining the number of clusters in a data set. *Psychometrika* 50(2):159–179.

Supplementary Method 2: **Source localization standardization**

After the inverse solution matrix has been applied to the ongoing EEG at each time point, a standardization of the estimated current density across time was applied to each solution point. As a matter of fact, substantial variability of power is observed across solution points when localizing the sources on ongoing (non-averaged) EEG in individual subjects (*Supplementary Figure S6).* These variations are supposed to come from some geometrical and mathematical approximations that are done during the inverse matrix calculation. It is thus necessary to find a way to correct for this power variability, in order to correctly estimate the fluctuations of brain activity over time in individual subjects and to compare them between subjects (*Supplementary Figure S6).*

The main idea here is to use the background activity of the norm of the inverse solution over time to estimate a baseline and a scaling factor for each solution point. In order to have a robust estimation, a large enough time sample should be used, preferably the whole recording as it was done in this study. Still, the correction factors can be satisfactorily computed on as little as a thousand time points, as long as no solution point remains in the same stable state more than half of the sampled time.

Here is a step-by-step description of this specialized standardization:

Given a 3D dipole (sp_x, sp_y, sp_z) at a given solution point sp, we define sp_χ as the squared value of its norm (Equ. 1). It therefore follows a Chi-square distribution of degree 3 for the noisy part of the data. The Chi-square variable sp_χ can be transformed into a normally distributed variable sp_N (Equ. 2) (1). Having now a normal distribution, it can be standardized into sp_Z by using the regular z-transform (Equ. 3). However, the values of μ and σ used for the z-transform have to be calculated only on the noisy part of the data - the background activity from the Chi-square i.e. the lowest values of the distribution. Hence μ is estimated from the left-most Mode of the sp_N distribution (Equ. 4). For the same reason, σ is estimated from the Median of Absolute Deviation (MAD), centred on the previously estimated μ, and computed only with the values below μ (Equ. 5). Implementation-wise, these estimators are computed multiple times on random sub-samplings of the data, and the two respective medians of all these estimators are finally taken.

Finally, because we started with positive data (the norm of a dipole), we also wish to end up with positive data, as to avoid any confusion due to having signed results. We define sp_{Z+} as sp_Z shifted by 3 standard deviations to the right, then divided by 3 so that the background mode is finally aligned to 1 (Equ. 6).

$$sp_{\chi} = {sp_x}^2 + {sp_y}^2 + {sp_z}^2 \quad \text{(Equ. 1)}$$

$$sp_N = \left(sp_{\chi}/3\right)^{1/3} \quad \text{(Equ. 2)}$$

$$sp_Z = \left(sp_N - \mu_{sp_N}\right)/\sigma_{sp_N} \quad \text{(Equ. 3)}$$

$$\mu_{sp_N} = \widehat{Mode}_{left}(sp_N) \quad \text{(Equ. 4)}$$

$$\sigma_{sp_N} = \widehat{MAD}_{left}(sp_N) \quad \text{(Equ. 5)}$$

$$sp_{Z+} = \max\left((sp_Z + 3)/3, 0\right) \quad \text{(Equ. 6)}$$

The result of this standardization procedure is comparable powers of the current density across all solution points, and a Normal distribution of the said solution points (*Supplementary Figure,* Fig. S6).

Reference:

1. Wilson B, Hilferty M (1931) The distribution of Chi-Square. *PNAS* 17(x):684–688.

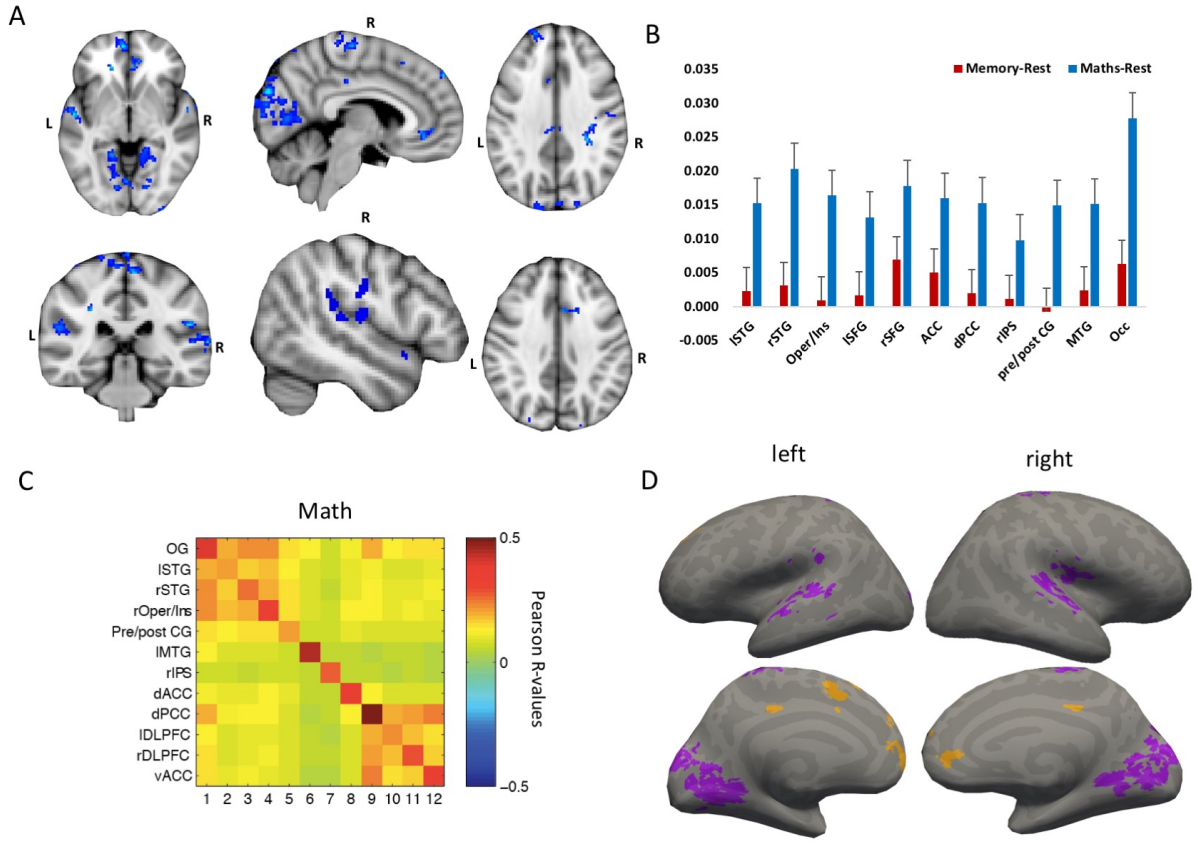

SFig. 1. Math-specific changes in fMRI activity and fMRI functional connectivity networks.
A. fMRI fALFF analysis. T-test of fALFF for math > memory condition revealed stronger activity in a set of brain areas. In the frontal lobe, significantly higher activity was found in the ventral and dorsal anterior cingulate cortex (vACC, BA24; dACC, BA32), and bilaterally in the superior frontal gyrus (lrSFG, BA32). Areas in the temporal lobe included bilaterally the superior temporal lobe (lrSTG, BA22), the left middle temporal gyrus (lMTG, BA21), and the right opercular cortex (rOperc, BA45). In the parietal cortex, significantly higher activity was found in the intraparietal sulcus (IPS, BA7) and the pre/post central gyrus (pre/postCG, BA3,1). The occipital findings concerned the occipital gyrus bilaterally (OCG, BA19). T-score maths > memory threshold: T>2.20; FDR-corrected for multiple comparisons (5%). **B. Areas of stronger activity in the math, compared to memory condition.** In contrast to the above observation of areas de-activated during math (compared to the rest condition), none of the areas with significantly higher activity in math compared to memory were actually de-activated during the memory condition. **C. Connectivity analysis.** The connectivity analysis revealed two distinct networks within the regions that had displayed stronger activity during the math condition: network III included the lrSTG, rOper/Ins, pre/post CG and OCG, while network IV comprised the dPCC, lrDLPFC, vACC. Beyond their strong intrinsic connections, the two networks were also moderately connected to each other, unlike what was observed for the memory-related networks. The lMTG and rIPS regions displayed no relevant correlations with any of the two networks, or with each other. **D. Sub-networks of the connectivity analysis.** The two identified networks were also projected onto a surface template for better visualization.

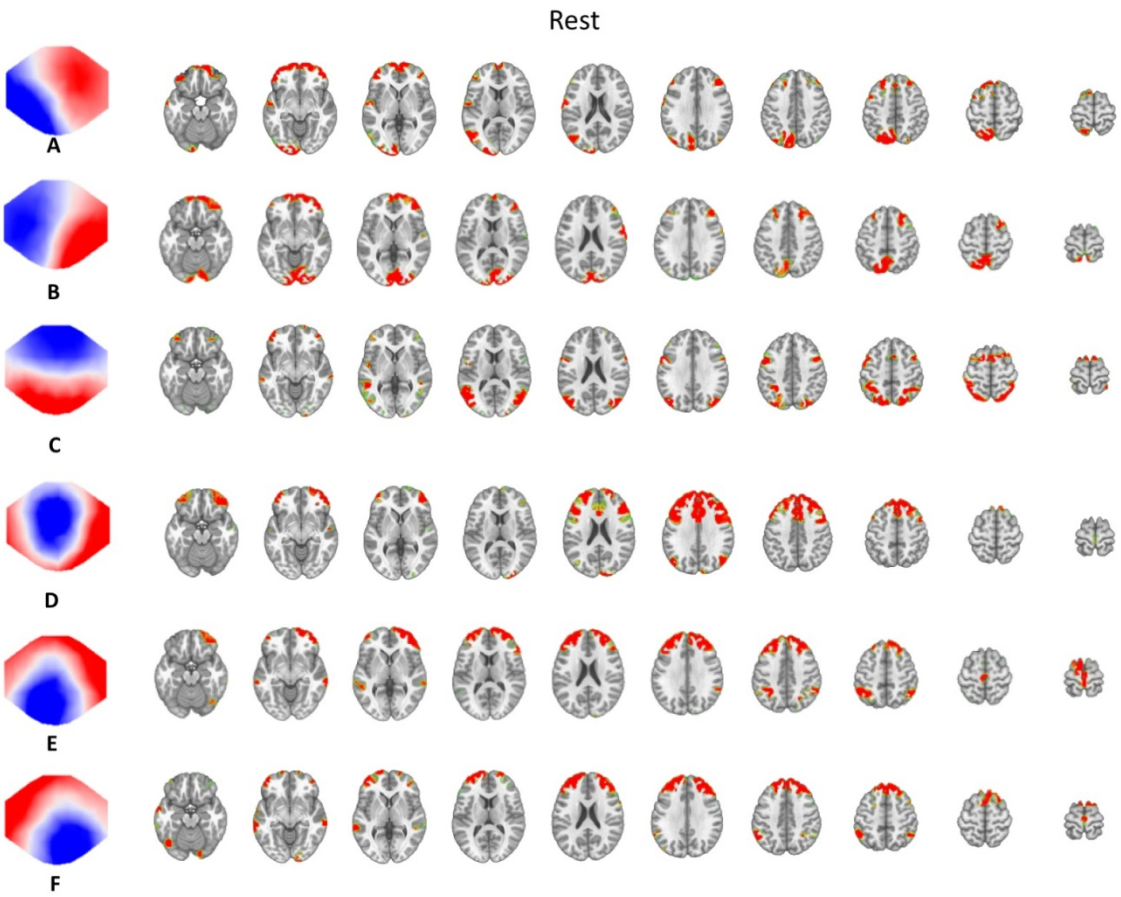

SFig. 2. Source localization of the six microstates during the rest condition. Sources are averaged across all time points that were labelled with the corresponding map and averaged across subjects. Areas with activity above 95 percentiles are shown.

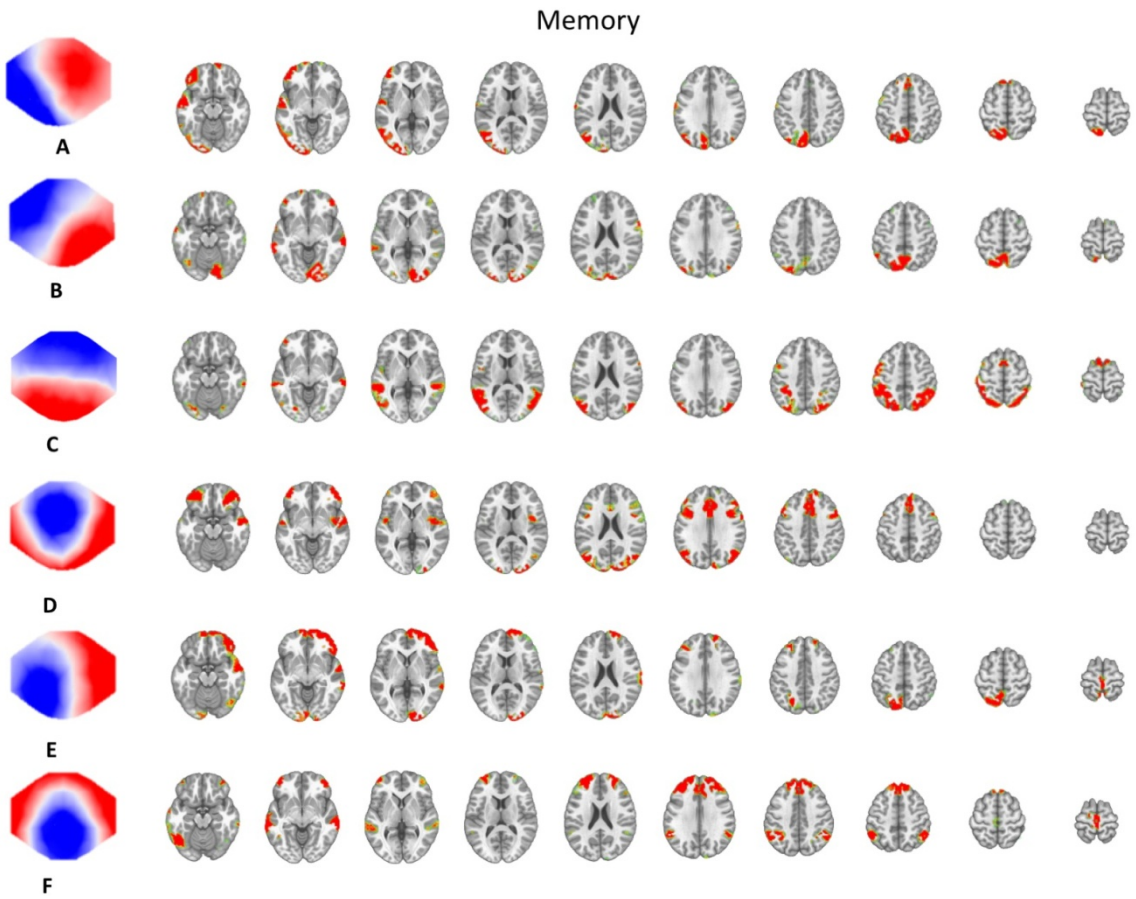

SFig. 3. Source localization of the six microstates during the memory condition. Sources are averaged across all time points that were labelled with the corresponding map and averaged across subjects. Areas with activity above 95 percentiles are shown.

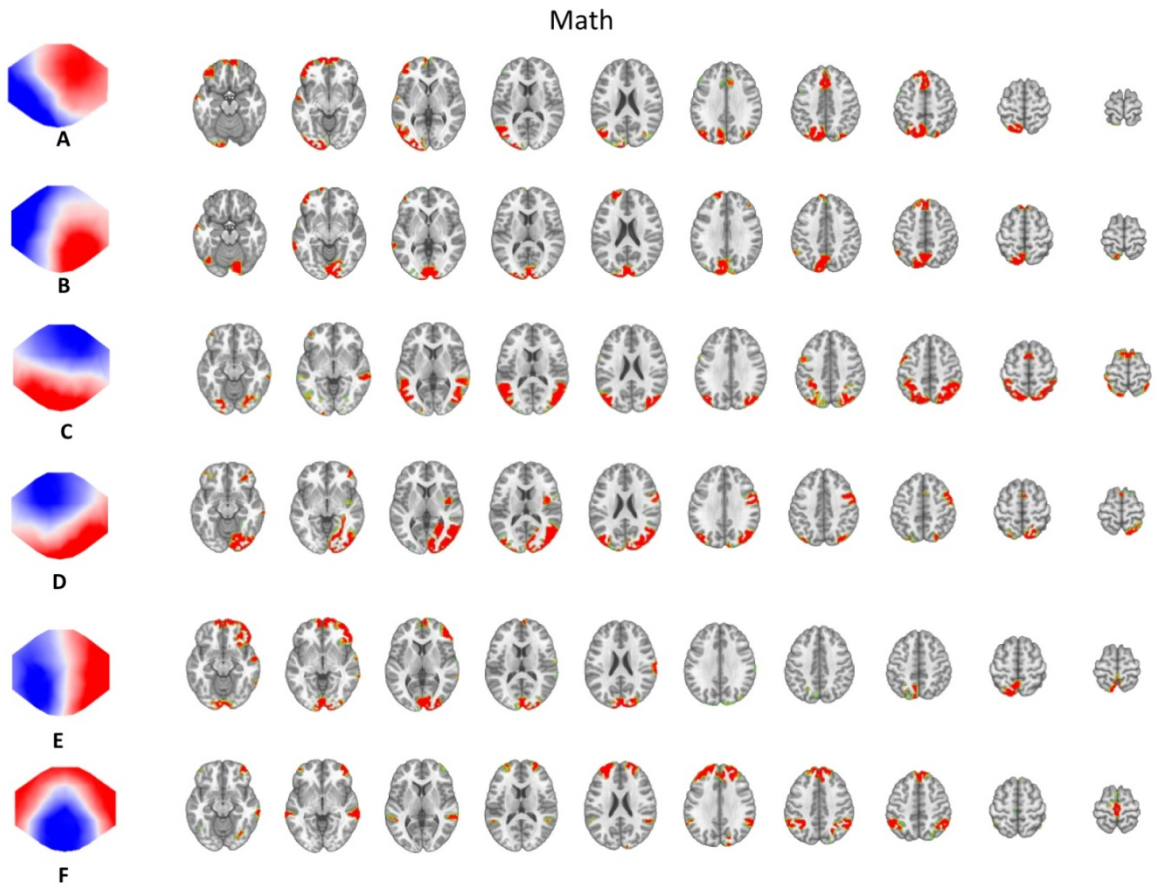

SFig. 4. Source localization of the six microstates during the math condition. Sources are averaged across all time points that were labelled with the corresponding map and averaged across subjects. Areas with activity above 95 percentiles are shown.

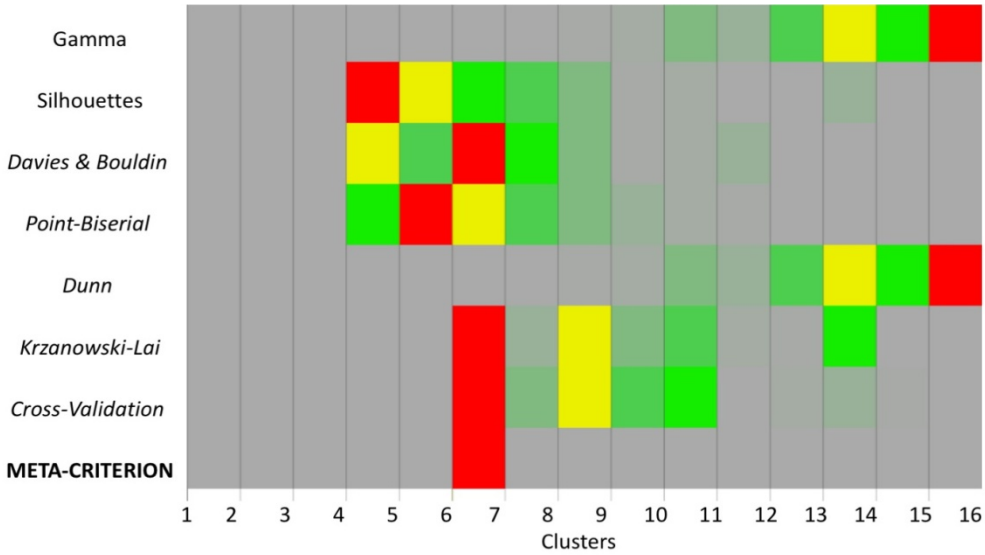

SFig. 5. Criteria for evaluating the optimal number of microstate maps
7 criteria (vertical axis) have been used to evaluate independently the quality of each clustering (horizontal axis). A red square points where a given criterion peaks, *i.e.* the optimal number of cluster for that criterion. The meta-criterion (last row) is defined as the median of all the optimal number of clusters across all criteria.

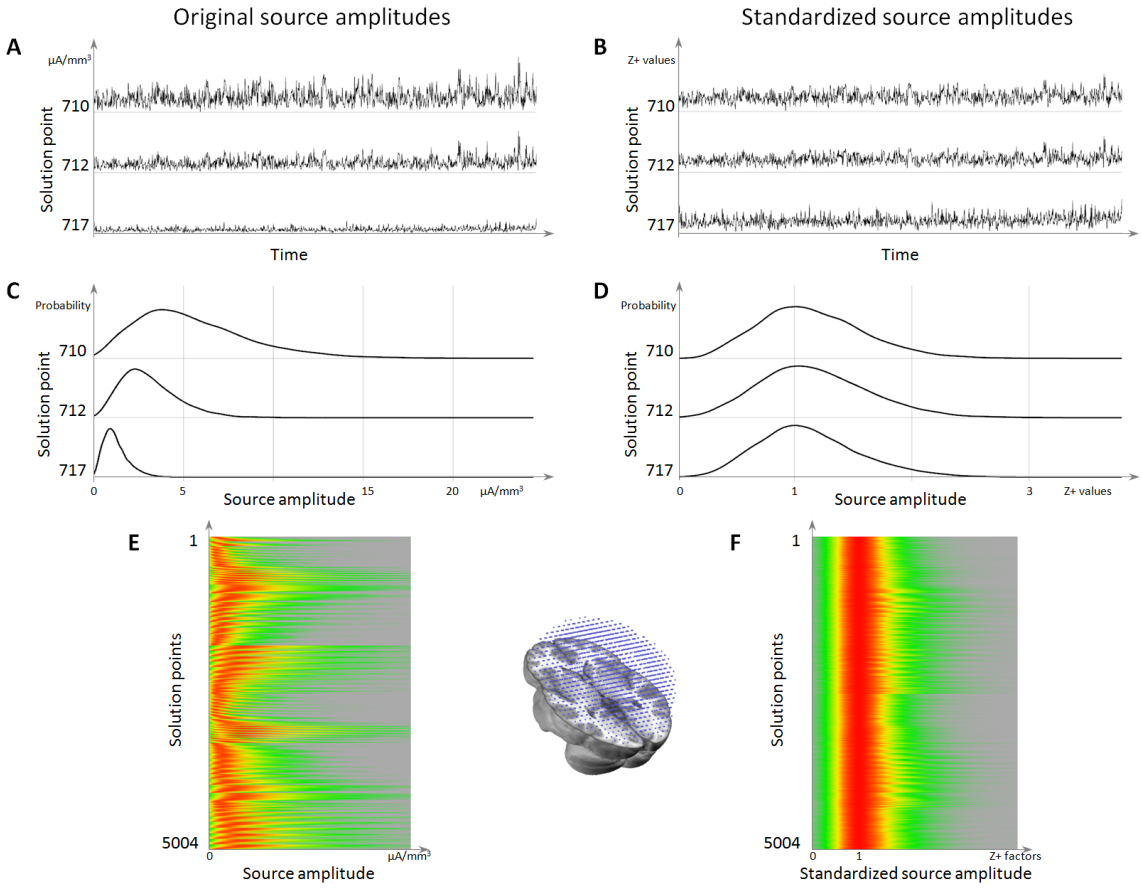

SFig. 6. Source localization standardization.
A. is the time series (horizontal axis) of 3 solution points (vertical axis), showing the difference in power range between them. **C.** is the histograms of these 3 solution points, showing that the background activity is the left-most mode of the distribution. **E.** is the histograms for all solution points (vertical axis), with the red color coding for the maximum probability. **B.** is the same time series as in **A** but after standardization, showing that the 3 solution points now have the same range. **D.** is the histograms after standardization, showing that all the background activity has been centered to 1. **F.** is all histograms after standardization, showing that all solution points now have a background range from 0 to 1, while retaining their respective highest activities.

MEMORY

MATH \ Microstate	A	B	C	D	E	F
A	NS 5	** 12	** 16	** 14	* 11	** 20
B	** 15	NS 7	** 18	** 17	* 11	** 16
C	* 10	* 11	NS 5	* 11	* 10	** 16
D	** 15	NS 7	** 14	NS 9	* 10	** 16
E	** 14	** 12	** 16	** 14	NS 6	** 24
F	** 14	NS 9	** 15	* 11	*** 12	NS 7

MEMORY

REST \ Microstate	A	B	C	D	E	F
A	NS 5	* 10	* 11	** 12	* 10	** 13
B	** 13	NS 6	* 11	** 12	NS 6	** 16
C	* 10	NS 8	NS 4	NS 8	NS 9	* 10
D	** 13	** 16	** 15	NS 7	** 17	* 11
E	** 14	** 12	** 12	* 11	* 10	* 9
F	** 13	* 9	** 13	** 12	** 13	NS 6

MATH

REST \ Microstate	A	B	C	D	E	F
A	NS 6	** 16	** 12	* 10	** 20	** 16
B	** 15	* 9	** 12	NS 8	NS 9	** 12
C	* 11	* 11	NS 7	* 11	NS 9	** 12
D	** 17	** 16	** 17	** 19	** 16	** 12
E	** 20	** 16	** 21	** 21	** 16	NS 7
F	** 14	** 13	** 16	** 17	* 21	NS 9

* p < .001 (T>9.5)
** p< .0001 (T>12)
Bonferroni corrected
Values = Tmax.

S Table1. Result of the T-test across subjects of the sources derived for each microstate in each of the three conditions. Significance values and maximal T-values are given. Note that in general the sources of the microstates with the same label are not significantly different, while the sources of different microstates are. An exception is microstate D and E in the comparison of the math vs. the rest condition. In this case all significantly different solution points for microstate D were located in the superior frontal gyrus where stronger activity was found in the rest condition.